

# UC Berkeley

## UC Berkeley Previously Published Works

### Title

Coexistence of octupole deformation and beta and gamma vibrational bands in  $^{148}\text{Ce}$

### Permalink

<https://escholarship.org/uc/item/22265027>

### Authors

Wang, EH

Brewer, NT

Hamilton, JH

et al.

### Publication Date

2021-11-01

### DOI

10.1016/j.nuclphysa.2021.122281

### Copyright Information

This work is made available under the terms of a Creative Commons Attribution-NonCommercial License, available at <https://creativecommons.org/licenses/by-nc/4.0/>

Peer reviewed

# Coexistence of octupole deformation and beta and gamma vibrational bands in $^{148}\text{Ce}$

E. H. Wang<sup>a</sup>, N. T. Brewer<sup>a</sup>, J. H. Hamilton<sup>a</sup>, A. V. Ramayya<sup>a</sup>, W. A. Yzaguirre<sup>a</sup>, J. K. Hwang<sup>a</sup>, S. H. Liu<sup>a</sup>, Y. X. Luo<sup>b</sup>, J. O. Rasmussen<sup>b</sup>, S. J. Zhu<sup>c</sup>, G. M. Ter-Akopian<sup>d</sup>, Yu. Ts. Oganessian<sup>d</sup>

<sup>a</sup>*Department of Physics and Astronomy, Vanderbilt University, Nashville, TN 37235, USA*

<sup>b</sup>*Lawrence Berkeley National Laboratory, Berkeley, CA 94720, USA*

<sup>c</sup>*Department of Physics, Tsinghua University, Beijing 100084, People's Republic of China* <sup>d</sup>*Joint Institute for Nuclear Research, RU-141980 Dubna, Russian Federation*

---

## Abstract

From  $\gamma$ - $\gamma$ - $\gamma$  and  $\gamma$ - $\gamma$ - $\gamma$ - $\gamma$  coincidence studies of spontaneous fission of  $^{252}\text{Cf}$ , new high spin states in  $^{148}\text{Ce}$  were identified. The octupole bands with  $s=+1$  and  $s=-1$  are expanded with spins with  $28^+$  and  $18^-$ , respectively. Importantly, a  $1\gamma$  vibrational band has been established up to  $14^+$  and a  $1\beta$  vibrational band up to  $6^+$ . The levels in  $\gamma$  and  $\beta$  bands in  $^{148}\text{Ce}$  are compared systematically to those in neighbouring  $^{150}\text{Nd}$  and  $^{152}\text{Sm}$  isotones. This comparison informs the role of deformation and shape transition in this mass region. New  $3^-$  and  $5^-$  members of the  $s=+1$  octupole band were observed.

*Keywords:* High-spin states, Gamma vibration,  $^{252}\text{Cf}$ , Beta vibration, Octupole correlation,  $^{148}\text{Ce}$

---

## 1. Introduction

Neutron-rich  $^{148}\text{Ce}$  nucleus lies well in the  $A \approx 150$  quadrupole and octupole deformed region. For octupole nuclei, a simplex quantum number  $s=PR^{-1}$  is usually used to characterize the level pattern. Here  $P$  is the parity operator and  $R$  is the signature operator which is a rotation by  $180^\circ$  to the principle axis. For even-even nuclei, there will be two sets of parity doublet bands with  $s = \pm 1$  corresponding to the two sequences following  $I^\pi = 0^+, 1^-, 2^+, 3^-, \dots$  ( $s = +1$ ) and  $I^\pi = 0^-, 1^+, 2^-, 3^+, \dots$  ( $s = -1$ ), respectively. While for odd- $A$  nuclei,

there are also two sets of bands with  $s = \pm i$  corresponding to  $I^\pi = 1/2^+, 3/2^-, 5/2^+, 7/2^-, \dots$  ( $s = i$ ) and  $I^\pi = 1/2^-, 3/2^+, 5/2^-, 7/2^+, \dots$  ( $s = -i$ ), respectively. In the  $A \sim 150$  region, nuclei are located between spherical and axial deformed shapes and are close to the predicted  $Z=56$  and  $N=88$  stable octupole island [1]. Quadrupole  $\gamma$  and  $\beta$  vibrational bands appear frequently. High spin states of nuclei in this region can provide important tests of nuclear models far from stability. Up until now in this region, one phonon  $\gamma$  and  $\beta$  vibrational bands were reported in  $^{146}\text{Ce}$  [2],  $^{148,150}\text{Nd}$  [3, 4],  $^{152}\text{Sm}$  [5] and some other even-even nuclei. In addition,  $\gamma$  soft bands have been reported from Te up to Ce isotopes [6, 7, 8]. Octupole deformation has been confirmed in Xe, Ba, La, Ce isotopes [9, 10, 11, 12, 13, 14, 15, 16, 17, 18, 19, 20, 21, 22, 23] by measuring prompt  $\gamma$ -rays following the spontaneous fission of heavy nuclei. In particular, first shape coexistence of quadrupole and octupole deformation was reported in Ref. [22]. As reported in Ref. [16],  $^{148}\text{Ce}$  was the first even-even nucleus with both the  $s=\pm 1$  octupole bands identified in this region. In this paper, we mainly present the newly identified one phonon  $\gamma$  and  $\beta$  vibrational bands, along with the octupole bands in  $^{148}\text{Ce}$ . Same raw data have been used from Ref. [16] while new four fold compilation and new analysis has been used in this paper.

## 2. Experimental setup

The experiment with  $^{252}\text{Cf}$  was carried out at the Lawrence Berkeley National Laboratory (LBNL). A  $62 \mu\text{Ci}$   $^{252}\text{Cf}$  source was sandwiched between two Fe foils of thickness  $10\text{mg}/\text{cm}^2$ . By using 101 Ge detectors of Gammasphere, the data were sorted into  $5.7 \times 10^{11}$   $\gamma$ - $\gamma$ - $\gamma$  and higher fold  $\gamma$  coincident events and  $1.9 \times 10^{11}$   $\gamma$ - $\gamma$ - $\gamma$ - $\gamma$  and higher fold  $\gamma$  coincident events. These  $\gamma$  coincident data were analyzed by the RADWARE software package [25]. Gamma-ray energies of the strong transitions have errors of 0.1 keV (same as the energy calibration error) [26] while the errors on the weak transitions could be as high as up to 0.5 keV.

### 3. Experimental results

The level scheme of  $^{148}\text{Ce}$  obtained in the present work is shown in Fig. 1. In previous  $^{252}\text{Cf}$  spontaneous fission (SF) studies, the ground state band was extended up to  $22^+$  and  $s=\pm 1$  octupole correlated bands were identified [16]. Those previously reported octupole bands are extended in the current level scheme in Fig. 1. New transition are labeled in red and with an asterisk. The  $22^+$  to  $20^+$  625 keV transition in the ground state band reported in Ref. [16] is replaced by a new 574.9 keV transition. The evidence for this transition can be found in Fig. 2, where a spectrum triple gated on the 559.8, 576.4 and 619.4 keV ground state band transitions is shown, expanded in the energy region of interest. In this spectrum, one can clearly see the 574.9 and 528.3 keV transitions and a weaker 572.4 keV transition on the left side of the 574.9 keV one. The intensities of these three transitions in this spectrum together with other coincidence spectra provide evidence of their order in the level scheme.

Fig. 3 depicts a triple gated coincidence spectra on the 353.2, 444.6 and 536.3 keV transitions in the  $s=-1$  octupole structure. In this spectrum, the new 648.4 keV transition on top of the band and the 600.9 keV linking transition to the  $7^-$  level of the  $s=1$  octupole band can be seen. The 648 keV transition is also seen in the 444-536-611 keV gate. Thus, this transition is populating the 3900 keV level. The 600 keV transition is not seen in the 167-353-444 keV gate. Therefore, it is depopulating the 1954 keV level.

Fig. 4 and 5 show evidence for the new linking transitions from the  $\gamma$  band to the ground state band. In Fig. 4 part (a), by gating on the 158.7 and 295.2 keV ground state band transitions, one can see the peaks of the previously identified 770.9 and new 926.3 and 1131.7 keV transitions populating the  $4^+$  state of the ground state band, the previously identified 948.9 and the new 745.1 keV transitions populating the  $6^+$  state of the ground state band, and the previously identified 804.7 and the new 913.3 keV transitions populating the  $8^+$  state of the ground state band. The transitions populating the  $4^+$  state are not seen in the 295 and 386 keV gate. The transitions populating the  $6^+$

state are not seen in the 386 and 451 keV gate. In addition, the new 586.4 keV transitions decaying from the  $5^-$  state of the  $s=+1$  octupole structure to the  $4^+$  state of the ground state band is also seen. Part (b) of Fig. 4 shows a double gated coincidence spectrum on the 386.1 and 512.8 keV transitions. In this spectrum, the previously identified 401.8 keV and the new 232.1, 436.1 and 600.9 keV transitions populating the  $7^-$  state of the  $s=1$  octupole structure can be seen. Fig. 5 denotes a  $\gamma$ -ray coincidence spectrum by gating on the 451.1 and 463.5 keV transitions. In this spectrum, the new 341.4 and 732.8 keV transitions decaying from the  $\gamma$  band to the  $9^-$  state of the  $s=1$  octupole structure can be seen. The new 552.2 keV transitions depopulating the 2307.3 keV  $10^-$  level can be also seen.

The spins and parities of the 1224.8 and 1585.1 keV levels in the  $\gamma$  band have been determined by angular correlation measurements. Details of this method can be found in Ref. [24]. More results about the angular correlations are discussed in the final part of this section. The  $0^+$ ,  $2^+$  and  $4^+$  levels in our  $1\beta$  vibrational band were previously reported in  $\beta^-$  decay of  $^{148}\text{La} \rightarrow ^{148}\text{Ce}$  [27] but not proposed as members of a  $\beta$ -vibrational band. These levels and the corresponding  $\gamma$  transitions are confirmed in the current work. A new 554.8 keV transition from a proposed ( $6^+$ ) member in this band was identified in the current work. Previously, levels forming a rotational band with 1789 keV band-head was reported in Ref. [16] without configuration assignment. In the current work, these levels are proposed to be members of a  $\gamma$ -vibrational band in  $^{148}\text{Ce}$ . The possible E2 transition from the 936.1 keV ( $2^+$ ) level to the ground state is not clearly seen in the  $^{100}\text{Zr}$  fission partner gate. Therefore, it is shown in a dashed line in the level scheme in Fig. 1. The possible E2 transition from the 990.0 keV ( $2^+$ ) level to the 770.5 keV ( $0^+$ ) level is not observed in the 379.3 and 611.8 keV double gate. The 936.1 keV level decays to  $2^+$  and  $4^+$  members of the ground band and is populated from the 1224.8 keV  $4^+$  state. Thus, this level can be firmly assigned as  $2^+$ . Note that usually, only M1, E1 and E2 transitions are observed in our data. Similarly, the 990.0 keV level can be assigned as  $2^+$  because this level decays to both the ground state and the 453.9 keV  $4^+$  state.

The  $\gamma$  ray intensities are listed in Table 1. The result combines the previous  $^{252}\text{Cf}$  SF work in Ref. [16] and new measurements in the current work. The intensities of the 482.0 keV transition (depopulating the the 936.1 keV level) and 536.1 keV (depopulating the 990.1 keV level) transitions can not be measured due to the high background from the 482.9 keV and 537.1 keV ones, respectively. The intensity of the 433.2 keV transition could not be measured but can be deduced from the branching ratio in Ref. [27]. Intensity of the 387.6 keV transition depopulating the 841.5 keV level could not be measured due to the strong 386.1 keV transition depopulating the 840.0 keV level, but can be deduced from the branching ratio in Ref. [27].

Angular correlations of successive  $\gamma$  ray transitions have been measured in order to assign spins and parities for the levels in  $^{148}\text{Ce}$  (Table. 2). The measured angular distribution curves are fitted to the following formula as listed in Ref. [24].

$$N(\theta) = A_0^{exp}(1 + A_2P_2(\cos(\theta)) + A_4P_4(\cos(\theta))) \quad (1)$$

In the equation,  $P_2$  and  $P_4$  refer to legendre polynomials. The  $\theta$  is the angle between two  $\gamma$  transitions. The fitted parameters are  $A_0$ ,  $A_2$  and  $A_4$ . Here  $A_0$  is a constant and  $A_2$  and  $A_4$  are used to compare with the theoretical values in order to determined the multipolarity of the transitions. A table of gamma-gamma angular correlation coefficients can be found in Ref. [28]. In our data, the most common transition types are M1 and E1 for dipole (D) and E2 for quadrupole (Q). Examples of the measured angular correlation curves of the 295.2-770.9 keV, 451.1-463.5 keV and 295.2-969.5 keV cascades are given in Fig. 6. The two different cascades of 969-295 keV and 363-969 keV provide consistent results for the mixing ratio of the 969.5 keV transition (9.6(1) and (14(10))). The table also shows an almost pure E2 character for the 663.0 keV transition linking the  $3^+$  1117.0 keV octupole band to the ground state band, as well as the 969.5 keV transition. The theoretical I to I-2 (quadrupole) and I-2 to I-3 (dipole) cascade and the I to I-1 (D) and I-1 to I-3 (Q) cascade both have  $A_2=-0.07$  and  $A_4=0$ . Thus, the results from 167-363, 353-167 and 463-

451 keV cascades are close to the theoretical pure I(D)I-1(Q)I-3, I(Q)I-2(D)I-3 and I(D)I-1(Q)I-3 types. Such measurements imply pure dipole (E1) character for the 167.1 and 463.5 keV transition. These values in Table. 2 support our spin and parity assignments for the octupole bands and  $\gamma$ -vibrational bands in  $^{148}\text{Ce}$ . More discussion of the basis of the  $\beta$  and  $\gamma$  vibrational bands are discussed below.

#### 4. discussion

The mixing ratios measured in the 770-295 keV and 745-386 keV cascades are 3.8(9) and 4.5(18), respectively, and represent >90% quadrupole (E2) component of the 770.9 and 745.1 keV transitions. As expected from the Bohr-Mottelson model, linking transitions from  $\gamma$ -vibrational bands to ground state bands are essentially pure E2. Such experimental evidence has been found in the  $\gamma$  band structure from  $^{150}\text{Sm}$  to  $^{184}\text{W}$  [29], and from  $^{102}\text{Mo}$  to  $^{116}\text{Pd}$  [30] regions.

The assignments of the  $2^+$  levels in the  $\beta$  and  $\gamma$  vibrational band is uncertain. Both 936.1 and 990.1 keV  $2^+$  levels do not decay to the 770.5 keV  $0^+$  level. Thus, these two  $2^+$  level could be switched around in these bands. Branching ratios of the 936.1 ( $2^+$ ), 990.1 ( $2^+$ ) and 1369.3 keV ( $4^+$ ) levels are listed in Table 3. The intensity ratios come from the  $^{148}\text{La}$   $\beta$  decay work [27]. In this table, the 936.1 and 990.1 keV levels have similar  $I(2^+ \rightarrow 4^+_{gs})/I(2^+ \rightarrow 2^+_{gs})$  intensity ratios. Nevertheless, according to the Alaga rules [31], the  $B(E2, 2^+ \rightarrow 4^+_{gs})/B(E2, 2^+ \rightarrow 2^+_{gs})$  ratio of a  $2^+_{1\beta}$  level should be much larger than that of the  $2^+_{1\gamma}$  one. The  $B(E2)$  ratio of the 1369.3 keV level is  $B(E2, 433.2)/B(E2, 379.3) = 0.14(2)$ . The 1224.8 keV  $4^+_{1\gamma}$  level does not decay to the 990.1 keV level. On the other hand, angular correlation measurements in Table 3 show some more evidence. The 777-158 angular correlation agrees with a pure dipole for the 777 keV  $2^+ \rightarrow 2^+_{gs}$  transition ( $\delta=0.13$ , 98% dipole). If  $2\sigma$  large error is taken, the mixing ratio can lead to  $\delta=3.3$  with 92% quadrupole. The angular correlation measurement of the 831-158 keV cascade dedicates  $\delta=5.5$  with 97% quadrupole for the 831.3

keV one, which is almost pure quadrupole for this  $2^+ \rightarrow 2^+_{gs}$  transition. Thus, the angular correlations indicate that the 990.1 keV level is likely to be the  $2^+$  member of the  $1\gamma$  band and the 936.1 keV level is the  $2^+$  member of the  $1\beta$  band. If the 936.1 keV level is assigned to the  $1\beta$  band, as labeled in the current level scheme in Fig. 1, the energy spacing between the  $2^+$  and  $0^+$  levels in  $1\beta$  band are close to the ground state band  $2^+$  and  $0^+$  energy spacing, and agrees better with the systematics in the neighboring  $^{146}\text{Ce}$ ,  $^{150}\text{Nd}$ ,  $^{152}\text{Sm}$  nuclei. However, since the experimental evidence is not sufficient enough and the mixing among the ground state band, the  $1\beta$  vibrational band and the  $1\gamma$  vibrational band is unknown, more theoretical work is needed to study the  $2^+$  level assignments of the  $1\beta$  and  $1\gamma$  band.

The level scheme of  $^{148}\text{Ce}$  is similar to those in  $^{150}\text{Nd}$  and  $^{152}\text{Sm}$  (see in Fig. 7). Such kind of similarity supports our assignments of the  $1\gamma$  and  $1\beta$  vibrational bands in  $^{148}\text{Ce}$ . These nuclei lie in the region between spherical and rigid deformed shapes. Note that according to the finite-range liquid-drop model (FRLDM) calculations [32],  $^{148}\text{Ce}$  has deformation parameters  $\epsilon_2=0.19$ ,  $\epsilon_3=0.05$ ,  $\epsilon_4=-0.05$ . The  $^{150}\text{Nd}$  and  $^{152}\text{Sm}$  nuclei were proposed to have X(5) dynamical symmetry, which corresponds to the critical point of the phase transition between spherical vibrator and axially deformed rotor [4, 33]. The  $^{148}\text{Ce}$  was also proposed to have X(5) symmetry in Ref. [34]. Zhang *et al.* introduced a F(5) scheme under Euclidean dynamical symmetry to calculate level energies and branching ratios of  $^{148}\text{Ce}$  and  $^{150}\text{Nd}$  [35]. However, the octupole correlations in  $^{148}\text{Ce}$  might interfere with the X(5) symmetry and weaken it compared to  $^{150}\text{Nd}$  and  $^{152}\text{Sm}$ .

The aligned angular momentum vs. rotation frequency is shown in Fig. 8. For the ground state band, a small upbending begins at about  $\hbar\omega \sim 0.29$  MeV. Then another strong bending occurs at  $\hbar\omega \sim 0.31$  MeV. These bending phenomena may originated from the alignment of a pair of  $h_{11/2}$  protons or a pair of  $i_{13/2}$  neutrons. The behavior of the  $\gamma$  band is more irregular. A pronounced backbending occurs at  $\hbar\omega \sim 0.25$  MeV roughly between the  $8^+$  and  $9^+$  levels. A similar back bend is observed in the  $1\gamma$  band in  $^{152}\text{Sm}$  between  $10^+$  and  $11^+$ .



This backbending in the  $\gamma$  band might be caused by the alignment of a pair of neutrons or admixture of octupole correlation. However, as discussed above, similar X(5) symmetry refers to an unstable  $\gamma$  vibration and might be quenched at higher spin.

Systematics of the octupole correlation and bands in  $^{144,146,148}\text{Ce}$  have been compared in Ref. [16]. The average  $B(E1)/B(E2)$  values were reported as  $0.82 \times 10^{-6} \text{ fm}^{-2}$  for the  $s=+1$  band, and  $1.51 \times 10^{-6} \text{ fm}^{-2}$  for the  $s=-1$  band [16]. In the current work,  $B(E1)/B(E2)$  values of the  $5^-$ ,  $7^-$ ,  $17^-$  states can be added as new transitions and levels in the  $s=+1$  band are identified. By using the expression in Ref. [16]. The  $B(E1)/B(E2)$  ratios are 0.001, 0.13 and  $0.4 \times 10^{-6} \text{ fm}^{-2}$  for the  $5^-$ ,  $7^-$ ,  $17^-$  states in the  $3^-$  841.5 keV band. With the new intensity measurements, the average  $B(E1)/B(E2)$  will decrease from 0.82 to  $0.55 \times 10^{-6} \text{ fm}^{-2}$  by 15% for the  $s=+1$  band, and 1.51 to 1.04 for the  $s=-1$  band. Such variation does not change the conclusion of octupole correlations reported in Ref. [16].

Comparison of the  $\gamma$  band with the negative parity component of the  $s=-1$  band shows that while at low spin values the trend of this line more closely resembles the trend of the  $\beta$  band, at higher spin the  $\gamma$  band trends according to the octupole band. Even though no transitions are reported between these bands to indicate mixing between these collective modes, this similarity seems to be an indication that octupole correlations in the  $\gamma$  band may be the more likely cause of this backbending. The drop of  $D_0$  with increasing  $N$  was found in both Ba and Ce isotopes [9, 36, 37, 38]. Such drop of  $D_0$  was reproduced by using reflection-asymmetric mean field shell correction theory [39, 40]. It is consistent with the available evidence to assert that the octupole states in  $^{148}\text{Ce}$  are more mixed with other degrees of freedom than those in  $^{144}\text{Ba}$ .

## 5. Summary

The coexistence of  $\beta$  band,  $\gamma$  bands and  $s=\pm 1$  octupole bands have been identified for the first time in the  $^{148}\text{Ce}$  nucleus in the  $A \sim 150$  octupole deformed

region. The previous  $s=\pm 1$  octupole bands have been extended. The  $\beta$  and  $\gamma$  vibrational bands have been observed. The  $\gamma$  band and the ground state band show irregular behavior of angular momentum alignment. Such phenomenon requires further theoretical interpretation.

### Acknowledgments

The work at Vanderbilt University and Lawrence Berkeley National Laboratory are supported by the US Department of Energy under Grant No. DE-FG05-88ER40407 and Contract No. DE-AC02-05CH11231. A post retirement association with Ramjas College, University of Delhi is acknowledged. The work at Tsinghua University was supported by the National Natural Science Foundation of China under Grant No. 11175095. The work at JINR was supported by the Russian Foundation for Basic Research Grant No. 08-02-00089 and by the INTAS Grant No. 03-51-4496.

### References

- [1] W. Nazarewicz and S.L. Tabor, Phys. Rev. C **45**, 2226 (1992).
- [2] T. Sharshar, S. Yamada, K. Okano, K. Aoki, Z. Phys. A **345**, 377 (1993).
- [3] R. W. Ibbotson, C.A. White, T. Czosnyka, R.A. Butler, N. Clarkson, D. Cline, R.A. Cunningham, M. Devlin, K.G. Helmer, T.H. Hoare, J.R. Hughes, G.D. Jones, A.E. Kavka, B. Kotlinski, R.J. Poynter, P.H. Regan, E.G. Vogt, R. Wadsworth, D.L. Watson and C.Y. Wu, Nucl. Phys. A **619**, 213 (1997).
- [4] R. Krücken, B. Albanna, C. Bialik, R. F. Casten, J. R. Cooper, A. Dewald, N. V. Zamfir, C. J. Barton, C. W. Beausang, M. A. Caprio, A. A. Hecht, T. Klug, J. R. Novak, N. Pietralla, and P. von Brentano, Phys. Rev. Lett. **88** 232501 (2002).

- [5] J. Konijn, J.B.R.Berkhout, W.H.A.hesselink, J.J.van Ruijven, P.van Nes, H.Verheul, F.W.N.de Boer, C.A.Fields, E.Sugarbaker, P.M.Walker and R.Bijker, Nucl. Phys. A **373**, 397 (1982).
- [6] A. J. Mitchell, C. J. Lister, E. A. McCutchan, M. Albers, A. D. Ayangeakaa, P. F. Bertone, M. P. Carpenter, C. J. Chiara, P. Chowdhury, J. A. Clark, P. Copp, H. M. David, A. Y. Deo, B. DiGiovine, N. D'Olympia, R. Dungan, R. D. Harding, J. Harker, S. S. Hota, R. V. F. Janssens, F. G. Kondev, S. H. Liu, A. V. Ramayya, J. Rissanen, G. Savard, D. Seweryniak, R. Shearman, A. A. Sonzogni, S. L. Tabor, W. B. Walters, E. Wang, and S. Zhu, Phys. Rev. C **93**, 014306 (2016).
- [7] W. Urban, K. Sieja, T. Rząca-Urban, M. Czerwiński, H. Naïdja, F. Nowacki, A. G. Smith, and I. Ahmad, Phys. Rev. C **93**, 034326 (2016).
- [8] H. Naïdja, F. Nowacki, B. Bounthong, M. Czerwiński, T. Rząca-Urban, T. Rogiński, W. Urban, J. Wiśniewski, K. Sieja, A. G. Smith, J. F. Smith, G. S. Simpson, I. Ahmad, and J. P. Greene, Phys. Rev. C **95**, 064303 (2017).
- [9] J. H. Hamilton, A.V.Ramayya, J.Zhu, G.M.Ter-Akopian, Yu.Ts.Oganessian, J.D.Cole, J.O.Rasmussen and M.A.Stoyer, Prog. Part. Nucl. Phys. **35**, 635 (1995).
- [10] S. J. Zhu, Q.H. Lu, J.H. Hamilton, A.V. Ramayya, L.K. Pekerbv, M.G. Wang, W.C. Ma, B.R.S. Babu, T.N. Ginter, J. Kormicki, D. Shi, J.K. Deng, W. Nazarewicz, J.O. Rasmussen, M.A. Stoyer, S.Y. Chu, K.E. Gregorich, M.F. Mohar, S. Asztalos, S.G. Prussin, J.D. Cole, R. Aryaeinejad, Y.K. Dardenne, M. Drigert, K.J. Moody, R.W. Loughed, J.F. Wild, N.R. Johnson, I.Y. Lee, F.K. McGowan, G.M. Ter-Akopian and Yu.Ts. Oganessian, Phys. Lett. **B357**, 273 (1995).
- [11] M. A. Jones, W. Urban, J.L. Durell, M. Leddy, W.R. Phillips, A.G. Smith, B.J. Varley, I. Ahmad, L.R. Morss, M. Bentaleb, E. Lubkiewicz, N. Schulz, Nucl. Phys. **A605**, 133 (1996).

- [12] S. J. Zhu, J. H. Hamilton, A. V. Ramayya, E. F. Jones, J. K. Hwang, M. G. Wang, X. Q. Zhang, P. M. Gore, L. K. Peker, G. Drafta, B. R. S. Babu, W. C. Ma, G. L. Long, L. Y. Zhu, C. Y. Gan, L. M. Yang, M. Sakhaee, M. Li, J. K. Deng, T. N. Ginter, C. J. Beyer, J. Kormicki, J. D. Cole, R. Aryaeinejad, M. W. Drigert, J. O. Rasmussen, S. Asztalos, I. Y. Lee, A. O. Macchiavelli, S. Y. Chu, K. E. Gregorich, M. F. Mohar, G. M. Ter-Akopian, A. V. Daniel, Yu. Ts. Oganessian, R. Donangelo, M. A. Stoyer, R. W. Lougheed, K. J. Moody, J. F. Wild, S. G. Prussin, J. Kliman, and H. C. Griffin, *Phys. Rev. C* **60**, 051304(R) (1999).
- [13] W. R. Phillips, I. Ahmad, H. Emling, R. Holzmann, R. V. F. Janssens, T. -L. Khoo, and M. W. Drigert, *Phys. Rev. Lett.* **57**, 3257 (1986).
- [14] W. Urban, W. R. Phillips, J. L. Durell, M. A. Jones, M. Leddy, C. J. Pearson, A. G. Smith, B. J. Varley, I. Ahmad, L. R. Morss, M. Bentaleb, E. Lubkiewicz, and N. Schulz, *Phys. Rev. C* **54**, 945 (1996).
- [15] Ts. Venkova, M. -G. Porquet, A. Astier, I. Deloncle, P. Petkov, A. Prévost, F. Azaiez, A. Bogachev, A. Buta, D. Curien, O. Dorvaux, G. Duchêne, J. Durell, B. J. P. Gall, M. Houry, F. Khalfallah, R. Lucas, M. Meyer, I. Piqueras, N. Redon, A. Roach, M. Rousseau, O. Stézowski and Ch. Theisen, *Eur. Phys. J. A* **26**, 315 (2005).
- [16] Y. J. Chen, S. J. Zhu, J. H. Hamilton, A. V. Ramayya, J. K. Hwang, M. Sakhaee, Y. X. Luo, J. O. Rasmussen, K. Li, I. Y. Lee, X. L. Che, H. B. Ding, and M. L. Li, *Phys. Rev. C* **73**, 054316 (2006).
- [17] H. J. Li, S. J. Zhu, J. H. Hamilton, A. V. Ramayya, J. K. Hwang, Z. G. Xiao, M. Sakhaee, J. Y. Guo, S. W. Chen, N. T. Brewer, S. H. Liu, K. Li, E. Y. Yeoh, Z. Zhang, Y. X. Luo, J. O. Rasmussen, I. Y. Lee, G. Ter-Akopian, A. Daniel, Yu. Ts. Oganessian, and W. C. Ma, *Phys. Rev. C* **86**, 067302 (2012).
- [18] H. J. Li, S. J. Zhu, J. H. Hamilton, E. H. Wang, A. V. Ramayya, Y. J. Chen, J. K. Hwang, J. Ranger, S. H. Liu, Z. G. Xiao, Y. Huang, Z. Zhang, Y. X.

- Luo, J. O. Rasmussen, I. Y. Lee, G. M. Ter-Akopian, Yu. Ts. Oganessian, and W. C. Ma, Phys. Rev. C 90, 047303 (2014).
- [19] Y. Huang, S. J. Zhu, J. H. Hamilton, E. H. Wang, A. V. Ramayya, Z. G. Xiao, H. J. Li, Y. X. Luo, J. O. Rasmussen, G. M. Ter-Akopian, and Yu. Ts. Oganessian, Phys. Rev. C 93, 064321 (2016).
- [20] E. H. Wang, W. Lewis, C. J. Zachary, J. H. Hamilton, A. V. Ramayya, J. K. Hwang, S. H. Liu, N. T. Brewer, Y. X. Luo, J. O. Rasmussen, S. J. Zhu, G. M. Ter-Akopian and Yu. Ts. Oganessian, Eur. Phys. J. A 53, 234 (2017).
- [21] J. Wisniewski, W. Urban, T. Rząca-Urban, A. G. Smith, J. F. Smith, G. S. Simpson, I. Ahmad, and J. P. Greene, Phys. Rev. C.96.064301(2017).
- [22] S.J.Zhu et al., Phys. Rev. Lett. 032501 (2020)
- [23] T. Rząca-Urban, W. Urban, J. A. Pinston, G. S. Simpson, A. G. Smith, and I. Ahmad, Phys. Rev. C 86, 044324 (2012).
- [24] A.V. Daniel, C. Goodin, K. Li, A.V. Ramayya, N.J. Stone, J.K. Hwang, J.H. Hamilton, J.R. Stone, Y.X. Luo, J.O. Rasmussen, M.A. Stoyer, S.J. Zhu, G.M. Ter-Akopian and I.Y. Lee, Nucl. Instrum. Methods B 262, 399 (2007).
- [25] D. C. Radford, Nucl. Instrum. Methods Phys. Res. A **361**, 297 (1995).
- [26] Y.X. Luo et al, Phys. Rev. C 64, 054306 (2001).
- [27] R.L.Gill, M. Shmid, R. E. Chrien, Y. Y. Chu, A. Wolf, D. S. Brenner, K. Sistemich, F. K. Wohn, H. Yamamoto, C. Chung, and W. B. Walters, Phys. Rev. C **27**, 1732 (1983).
- [28] H. W. Taylor et al., NUCLEAR DATA TABLES A9, 1-83 (1971).
- [29] J. Lange, Krishna Kumar and J. H. Hamilton, Rev. Mod. Phys. **54**, 119 (1982).

- [30] J.M. Eldridge, B. Fenker, J.H. Hamilton, C. Goodin, C.J. Zachary, E. Wang, A.V. Ramayya, A.V. Daniel, G.M. Ter-Akopian, Yu.Ts. Oganessian, Y.X. Luo, J.O. Rasmussen, and S.J. Zhu, *Eur. Phys. J. A* **54**, 15 (2018).
- [31] A.Bohr and B.R. Mottelson , *Nuclear Structure* vol. 1,2 (1969).
- [32] P. Möller, A.J. Sierk, R. Bengtsson, H. Sagawa and T. Ichikawa, *Atomic Data and Nuclear Data Tables* **98**, 149 (2012).
- [33] R.F. Casten and N. V. Zamfir, *Phys. Rev. Lett.* **87**, 052503 (2001).
- [34] L.J.Lv, *Journal of Chifeng University (Natural Science Edition)* **23**, 5 (2007).
- [35] Yu Zhang, Yu-Xin Liu, Feng Pan, Yang Sun, J.P. Draayer, *Physics Letters B* **732**, 55 (2014).
- [36] W.R. Phillips et al. *Phys. Rev. Lett* 57,3257 (1986).
- [37] W. Urban, M.A. Jones, J.L. Durell, M. Leddy, W.R. Phillips, A.G. Smith, B.J. Varley, I. Ahmad, L.R. Morss, M. Bentaleb, E. Lubkiewicz, N. Schulz, *Nucl. Phys. A* **613**, 107 (1997).
- [38] J.H. Hamilton *et al.*, *Highlights of Modern Nuclear Structure*, p 15 (Ed. A. Corvello). World Sci., Singapore 1998.
- [39] P.A. Butler and W. Nazarewicz, *Nucl. Phys. A* **533**, 249 (1991).
- [40] W. Nazarewicz and P. Olanders, *Nuclear Physics A* **441**(3), 420–444 (1985).

Table 1: The  $\gamma$  ray relative intensities of  $^{148}\text{Ce}$ . The  $\gamma$ -ray transition intensities are normalized to the 158.7 keV one. Some of the weak transition intensities are given as upper limits. New transitions are labeled with an asterisk. In this table,  $E_\gamma$ ,  $I_\gamma$ ,  $E_i$  (keV),  $I_i^\pi$ ,  $E_f$  (keV) and  $I_f^\pi$  refer to  $\gamma$ -ray energy,  $\gamma$ -ray intensity, initial level energy, initial level spin and parity, final level energy and final level spin and parity, respectively.

$E_\gamma$ (keV)	$I_\gamma$	$E_i$ (keV)	$I_i^\pi$	$E_f$ (keV)	$I_f^\pi$
54.1	<0.1	990.1	2 <sup>+</sup>	936.1	2 <sup>+</sup>
103.2	0.8(3)	2328.7	12 <sup>+</sup>	2225.8	11 <sup>-</sup>
104.7	1.9(2)	1787.0	7 <sup>+</sup>	1682.4	6 <sup>-</sup>
108.7	1.9(2)	2307.3	10 <sup>-</sup>	2198.7	9 <sup>+</sup>
109.2	<0.1	2204.4	(9 <sup>+</sup> )	2095.8	(8 <sup>+</sup> )
(134.8)		1224.8	4 <sup>+</sup>	1090.0	(3 <sup>+</sup> )
136.1	0.14(6)	2888.5	14 <sup>+</sup>	2752.5	13 <sup>-</sup>
137.8	0.3(1)	3464.9	16 <sup>+</sup>	3326.9	15 <sup>-</sup>
(155.3)	<0.3	1380.4	(5 <sup>+</sup> )	1224.8	4 <sup>+</sup>
158.7	100(5)	158.7	2 <sup>+</sup>	0.0	0 <sup>+</sup>
167.1	7.5(6)	1954.1	8 <sup>-</sup>	1787.0	7 <sup>+</sup>
(195.4)		1682.4	6 <sup>-</sup>	1486.8	4 <sup>-</sup>
198.6	0.24(4)	1040.2	5 <sup>-</sup>	841.5	3 <sup>-</sup>
203.8	2.4(3)	1788.9	(7 <sup>+</sup> )	1585.1	6 <sup>+</sup>
(204.3)	<0.3	1585.1	6 <sup>+</sup>	1380.4	(5 <sup>+</sup> )
232.3	1.0(1)	1585.1	6 <sup>+</sup>	1352.8	7 <sup>-</sup>
244.6	3.3(3)	2198.7	9 <sup>+</sup>	1954.1	8 <sup>-</sup>
252.2	0.3(1)	1369.3	(4 <sup>+</sup> )	1117.0	3 <sup>+</sup>
259.0	5.5(3)	1682.4	6 <sup>-</sup>	1423.4	5 <sup>+</sup>

(Continue on next page)

Table 1. (continued)

$E_\gamma$ (keV)	$I_\gamma$	$E_i$ (keV)	$I_i^\pi$	$E_f$ (keV)	$I_f^\pi$
271.6	2.0(2)	1954.1	8 <sup>-</sup>	1682.4	6 <sup>-</sup>
283.2	<0.1	2487.5	(10 <sup>+</sup> )	2204.4	(9 <sup>+</sup> )
288.8	0.24(5)	1224.8	4 <sup>+</sup>	936.1	2 <sup>+</sup>
290.4	~0.1	1380.4	(5 <sup>+</sup> )	1090.0	(3 <sup>+</sup> )
295.2	116(6)	453.9	4 <sup>+</sup>	158.7	2 <sup>+</sup>
306.4	2.1(2)	1423.4	5 <sup>+</sup>	1117.0	3 <sup>+</sup>
307.1	1.4(2)	2095.8	8 <sup>+</sup>	1788.9	7 <sup>+</sup>
312.5	0.04(1)	1352.8	7 <sup>-</sup>	1024.3	5 <sup>-</sup>
341.4	0.4(1)	2095.8	(8 <sup>+</sup> )	1754.6	9 <sup>-</sup>
353.2	6.3(9)	2307.3	(10 <sup>-</sup> )	1954.1	8 <sup>-</sup>
360.4	0.6(1)	1585.1	6 <sup>+</sup>	1224.8	4 <sup>+</sup>
363.6	6.4(4)	1787.0	7 <sup>+</sup>	1423.4	5 <sup>+</sup>
369.8	1.1(1)	1486.8	4 <sup>-</sup>	1117.0	3 <sup>+</sup>
379.3	0.8(1)	1369.3	(4 <sup>+</sup> )	990.1	2 <sup>+</sup>
383.2	~0.02	1423.4	5 <sup>+</sup>	1040.2	5 <sup>-</sup>
386.1	85(4)	840.0	6 <sup>+</sup>	453.9	4 <sup>+</sup>
387.6		841.5	3 <sup>-</sup>	453.9	4 <sup>+</sup>
391.6	0.7(1)	2487.5	(10 <sup>+</sup> )	2095.8	(8 <sup>+</sup> )
401.8	2.9(2)	1754.6	9 <sup>-</sup>	1291.1	7 <sup>-</sup>
(408.2)	<0.4	1788.9	(7 <sup>+</sup> )	1380.4	(5 <sup>+</sup> )
411.7	2.1(2)	2198.7	9 <sup>+</sup>	1787.0	7 <sup>+</sup>
415.3	0.2(1)	2204.4	(9 <sup>+</sup> )	1788.9	(7 <sup>+</sup> )
423.8	2.4(5)	2752.5	13 <sup>-</sup>	2328.7	12 <sup>+</sup>
433.2		1369.3	(4 <sup>+</sup> )	936.1	2 <sup>+</sup>
434.2	3.4(3)	2225.8	11 <sup>-</sup>	1791.6	10 <sup>+</sup>
436.1		1788.9	7 <sup>+</sup>	1352.8	7 <sup>-</sup>
438.4	0.7(1)	3326.9	15 <sup>-</sup>	2888.5	14 <sup>+</sup>
444.6	3.7(5)	2751.9	12 <sup>-</sup>	2307.3	10 <sup>-</sup>

(Continue on next page)



Table 1. (continued)

$E_\gamma$ (keV)	$I_\gamma$	$E_i$ (keV)	$I_i^\pi$	$E_f$ (keV)	$I_f^\pi$
451.1	54(3)	1291.1	8 <sup>+</sup>	840.0	6 <sup>+</sup>
453.8	0.7(3)	2652.5	(11 <sup>+</sup> )	2198.7	9 <sup>+</sup>
471.2	1.4(2)	2225.8	11 <sup>-</sup>	1754.6	9 <sup>-</sup>
463.5	5.7(3)	1754.6	9 <sup>-</sup>	1291.1	8 <sup>+</sup>
480.4	0.07(3)	3945.0	17 <sup>-</sup>	3464.9	16 <sup>+</sup>
482.1		936.1	2 <sup>+</sup>	453.9	4 <sup>+</sup>
482.9	0.4(1)	2970.4	12 <sup>+</sup>	2487.5	10 <sup>+</sup>
495.8	1.5(1)	1787.0	7 <sup>+</sup>	1291.1	8 <sup>+</sup>
497.8	<1	1788.9	7 <sup>+</sup>	1291.1	8 <sup>+</sup>
500.5	26(2)	1791.6	10 <sup>+</sup>	1291.1	8 <sup>+</sup>
510.7	0.3(1)	2095.8	(8 <sup>+</sup> )	1585.1	6 <sup>+</sup>
512.8	7.7(5)	1352.8	7 <sup>-</sup>	840.0	6 <sup>+</sup>
526.8	1.4(2)	2752.5	13 <sup>-</sup>	2225.8	11 <sup>-</sup>
528.3	0.15(7)	5789.2	(24 <sup>+</sup> )	5260.9	(22 <sup>+</sup> )
536.3	2.1(3)	3288.2	(14 <sup>-</sup> )	2751.9	12 <sup>-</sup>
536.5		990.1	2 <sup>+</sup>	453.9	4 <sup>+</sup>
537.1	18(1)	2328.7	12 <sup>+</sup>	1791.6	10 <sup>+</sup>
552.7	0.2(1)	2307.3	10 <sup>-</sup>	1754.6	9 <sup>-</sup>
554.8	0.3(1)	1924.1	(6 <sup>+</sup> )	1369.3	(4 <sup>+</sup> )
559.8	8.7(5)	2888.5	14 <sup>+</sup>	2328.7	12 <sup>+</sup>
572.4	0.06(4)	6361.6	(26 <sup>+</sup> )	5789.2	(24 <sup>+</sup> )
574.1	~0.1	3544.5	(14 <sup>+</sup> )	2970.4	(12 <sup>+</sup> )
574.6	1.1(2)	3326.9	15 <sup>-</sup>	2752.5	13 <sup>-</sup>
574.9	0.3(1)	5260.9	(22 <sup>+</sup> )	4686.0	(20 <sup>+</sup> )
576.4	4.0(2)	3464.9	16 <sup>+</sup>	2888.5	14 <sup>+</sup>
583.3	4.5(3)	1423.4	5 <sup>+</sup>	840.0	6 <sup>+</sup>
586.4	1.9(2)	1040.2	5 <sup>-</sup>	453.9	4 <sup>+</sup>
600.9	1.5(2)	1954.1	8 <sup>-</sup>	1352.8	7 <sup>-</sup>

(Continue on next page)

Table 1. (continued)

$E_\gamma$ (keV)	$I_\gamma$	$E_i$ (keV)	$I_i^\pi$	$E_f$ (keV)	$I_f^\pi$
601.7	1.9(3)	4066.6	(18 <sup>+</sup> )	3464.9	16 <sup>+</sup>
611.8	0.8(3)	3900.0	(16 <sup>-</sup> )	3288.2	(14 <sup>-</sup> )
611.9	0.4(1)	770.6	0 <sup>+</sup>	158.7	2 <sup>+</sup>
618.1	0.10(4)	3945.0	17 <sup>-</sup>	3326.9	15 <sup>-</sup>
619.4	1.0(2)	4686.0	(20 <sup>+</sup> )	4066.6	(18 <sup>+</sup> )
(636.1)	<0.1	1090.0	(3 <sup>+</sup> )	453.9	4 <sup>+</sup>
641.6	0.44(6)	2970.4	(12 <sup>+</sup> )	2328.7	12 <sup>+</sup>
648.4	0.3(1)	4548.4	(18 <sup>-</sup> )	3900.0	(16 <sup>-</sup> )
655.9	0.10(3)	3544.5	(14 <sup>+</sup> )	2888.5	14 <sup>+</sup>
662.5	1.2(1)	1954.1	8 <sup>-</sup>	1291.1	8 <sup>+</sup>
663.2	2.1(5)	1117.0	3 <sup>+</sup>	453.9	4 <sup>+</sup>
682.8	1.4(1)	841.5	3 <sup>-</sup>	158.7	2 <sup>+</sup>
695.9	2.6(3)	2487.5	(10 <sup>+</sup> )	1791.6	10 <sup>+</sup>
732.8	0.24(7)	2487.5	(10 <sup>+</sup> )	1754.6	9 <sup>-</sup>
744.3	0.21(3)	2970.4	(12 <sup>+</sup> )	2225.8	11 <sup>-</sup>
745.1	5.3(5)	1585.1	(6 <sup>+</sup> )	840.0	6 <sup>+</sup>
770.9	4.7(4)	1224.8	4 <sup>+</sup>	453.9	4 <sup>+</sup>
777.4	1.8(2)	936.1	2 <sup>+</sup>	158.7	2 <sup>+</sup>
804.7	2.6(2)	2095.8	(8 <sup>+</sup> )	1291.1	8 <sup>+</sup>
831.4	1.1(1)	990.1	2 <sup>+</sup>	158.7	2 <sup>+</sup>
913.3	0.11(4)	2204.4	(9 <sup>+</sup> )	1291.1	8 <sup>+</sup>
926.3	0.25(4)	1380.4	(5 <sup>+</sup> )	453.9	4 <sup>+</sup>
931.3	0.6(1)	1090.0	3 <sup>+</sup>	158.7	2 <sup>+</sup>
(935.9)	<0.4	936.1	2 <sup>+</sup>	0.0	0 <sup>+</sup>
946.7	4.2(4)	1787.0	7 <sup>+</sup>	840.0	6 <sup>+</sup>
948.9	2.5(3)	1788.9	(7 <sup>+</sup> )	840.0	6 <sup>+</sup>
958.3	4.7(3)	1117.0	3 <sup>+</sup>	158.7	2 <sup>+</sup>
969.5	10.0(5)	1423.4	5 <sup>+</sup>	453.9	4 <sup>+</sup>

(Continue on next page)

Table 2: Angular correlation for  $^{148}\text{Ce}$  measured in the present work. Here D,Q stand for dipole (M1 or E1) and quadrupole (E2) multipolarity of  $\gamma$ -ray transitions. The  $\delta$  represents mixing ratios.

cascade	decay pattern	$A_2/A_4$ values	$\delta$
663.0-295.2	$3^+(\text{D,Q})4^+(\text{Q})2^+$	0.05(5)/-0.24(8)	10(6)
969.5-295.2	$5^+(\text{D,Q})4^+(\text{Q})2^+$	-0.06(1)/-0.09(2)	9.6(1)
363.3-969.5	$7^+(\text{Q})5^+(\text{D,Q})4^+$	0.03(2)/-0.02(3)	14(10)
167.1-363.3	$8^-(\text{D})7^+(\text{Q})5^+$	-0.04(2)/-0.04(4)	
353.5-167.1	$10^-(\text{Q})8^-(\text{D})7^+$	-0.07(3)/-0.01(4)	
444.6-353.5	$12^-(\text{Q})10^-(\text{Q})8^-$	0.16(3)/0.03(5)	
536.1-444.6	$14^-(\text{Q})12^-(\text{Q})10^-$	0.08(3)/0.03(5)	
411.9-363.3	$9^+(\text{Q})7^+(\text{Q})5^+$	0.16(8)/0.15(14)	
777.2-158.7	$2^+(\text{D,Q})2^+(\text{Q})0^+$	0.15(8)/0.08(13)	0.13(11) 3.3(13), $2\sigma$
831.3-158.7	$2^+(\text{D,Q})2^+(\text{Q})0^+$	-0.20(6)/0.31(10)	5.5(35)
770.9-295.2	$4^+(\text{D,Q})4^+(\text{Q})2^+$	-0.02(2)/0.16(4)	3.8(9)
745.1-386.1	$6^+(\text{D,Q})6^+(\text{Q})4^+$	-0.07(2)/0.13(4)	4.5(18)
463.5-451.1	$9^-(\text{D})8^+(\text{Q})6^+$	-0.06(2)/-0.01(2)	

Table 1. (continued)

$E_\gamma$ (keV)	$I_\gamma$	$E_i$ (keV)	$I_i^\pi$	$E_f$ (keV)	$I_f^\pi$
990.1	1.3(1)	990.1	$2^+$	0.0	$0^+$
1066.4	0.7(1)	1224.8	$4^+$	158.7	$2^+$
(1131.7)	<0.7	1585.1	$6^+$	453.9	$4^+$
(1210.4)	<0.5	1369.3	( $4^+$ )	158.7	$2^+$

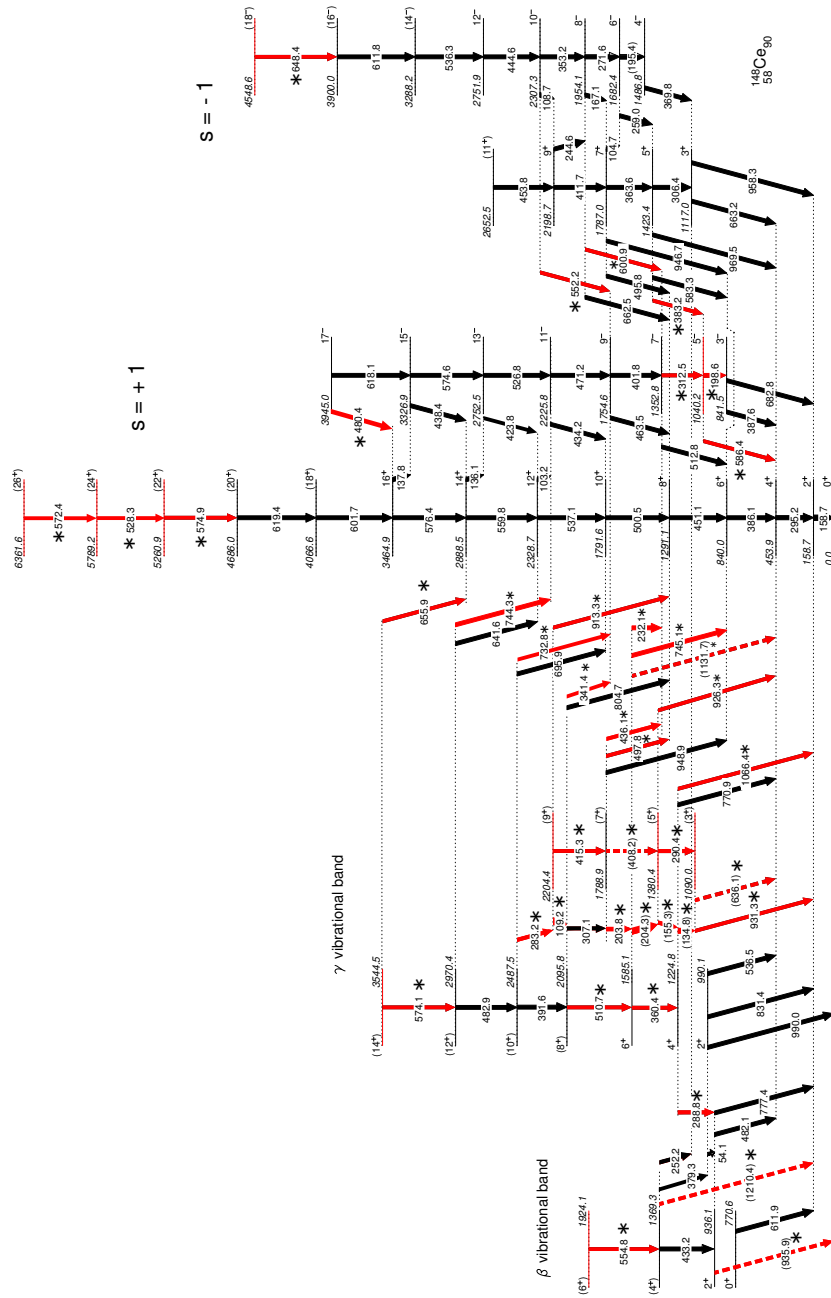


Figure 1: (Color online) Partial level scheme of  $^{148}\text{Ce}$ . New transitions in the current work are labeled in red and an asterisk. The 475 keV transition populating the 2199 keV level reported from Ref. [16] is replaced with a 453 keV transition. Transitions with dashed lines and parentheses are tentative.

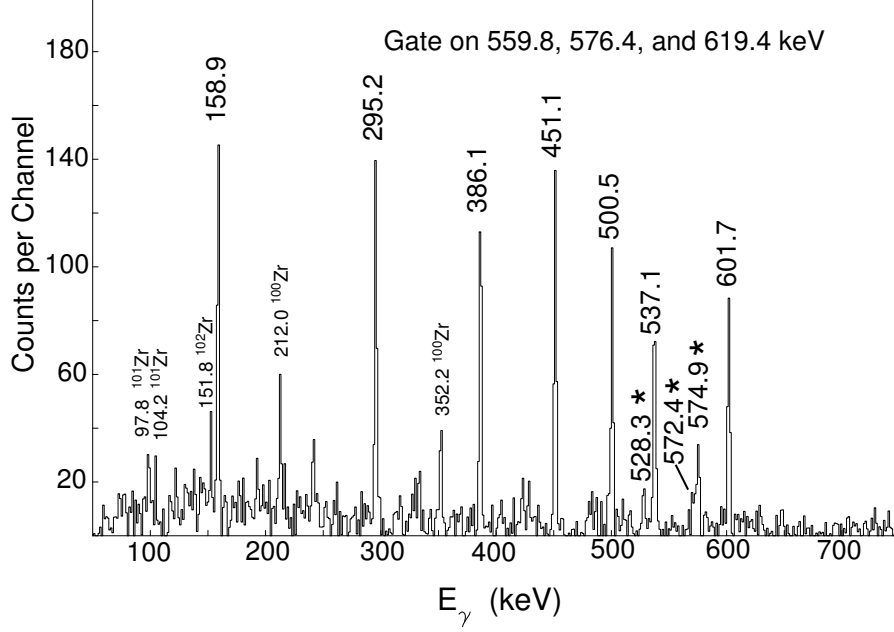


Figure 2: Triple gate of 559.8, 576.4 and 619.4 keV transitions showing evidence of the new 528.3, 572.4 and 574.9 keV transitions in the ground state band in  $^{148}\text{Ce}$ . New transitions are labeled with an asterisk.

Table 3: The partial  $\gamma$  ray branching ratio of  $^{148}\text{Ce}$ . Part of values come from Ref. [27].

$E_{level}$ (keV)	$E_{\gamma}$ (keV)	branchings	pattern
936.1	482.1	13(1)	$2^+ \rightarrow 4^+_{gs}$
	777.2	100(3)	$2^+ \rightarrow 2^+_{gs}$
990.1	54.1		$2^+ \rightarrow 2^+$
	536.1	5.3(6)	$2^+ \rightarrow 4^+_{gs}$
	831.3	55(3)	$2^+ \rightarrow 2^+_{gs}$
	990.1	100(3)	$2^+ \rightarrow 0^+_{gs}$
1369.3	379.3	100(10)	$4^+_{1\beta} \rightarrow 2^+$
	433.2	28.2(14)	$4^+_{1\beta} \rightarrow 2^+$

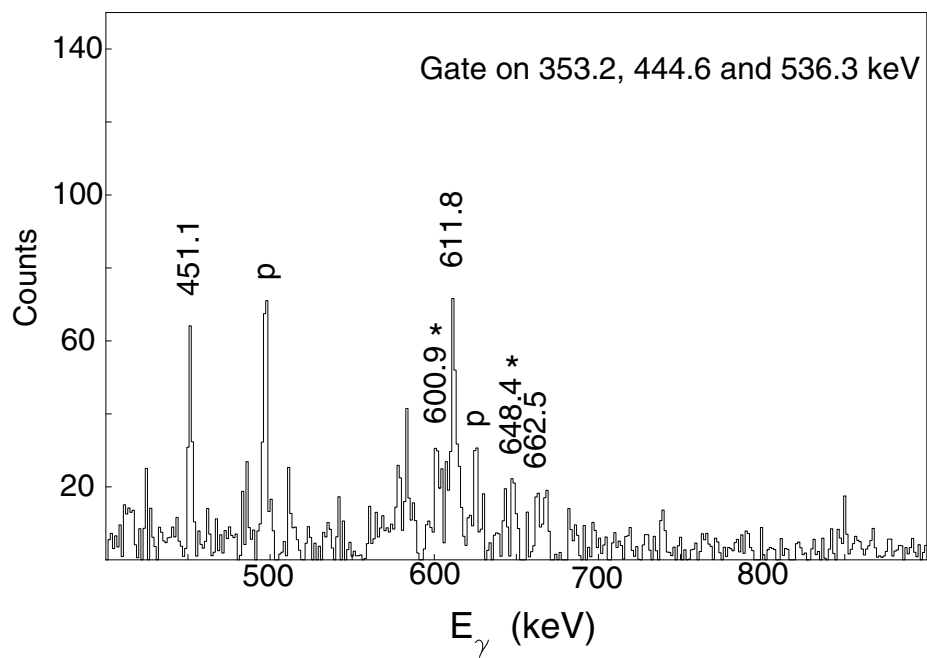


Figure 3: Triple gate of 353.2, 444.6 and 536.3 keV transitions showing evidence of the new 600.9 and 648.4 keV transitions in  $^{148}\text{Ce}$ . New transitions are labeled with an asterisk. The Zr fission partner transitions are labeled with a "p".

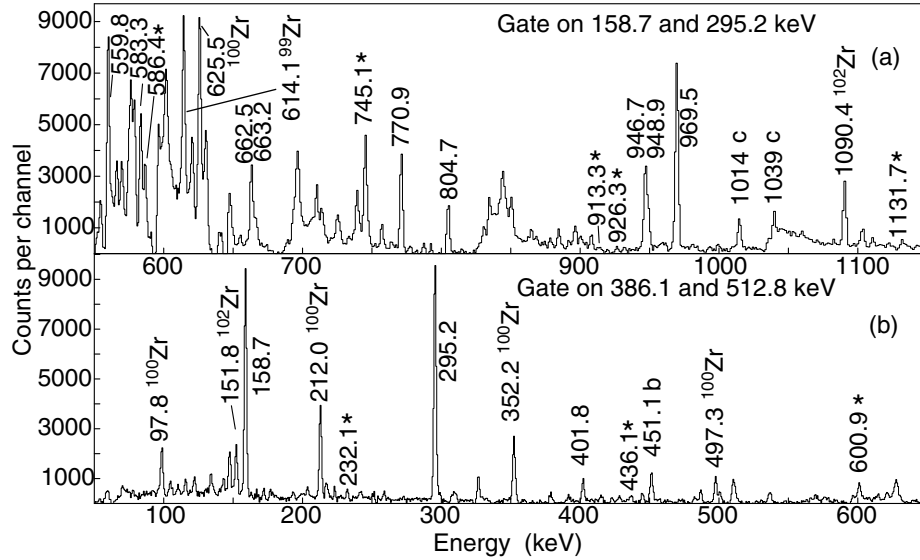


Figure 4: Partial coincidence spectra by gating on (a) 158.7 and 295.2 keV in the ground state band and (b) 386.1 and 512.8 keV transitions in  $^{148}\text{Ce}$ . New transitions are labeled with an asterisk. The 1014 and 1039 keV transitions labeled with a "c" in part (a) are neutron scatter peaks. The 451.1 keV ground state band transition labeled with a "b" in part (b) comes from the background coincidence of the 386.1 keV transition.

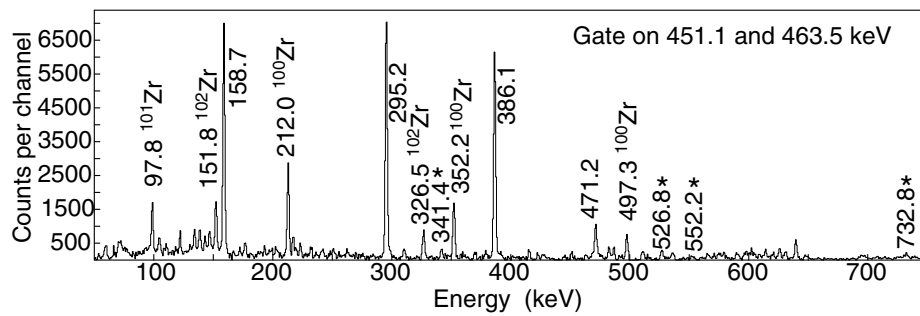


Figure 5: Partial double gate of 451.1 and 463.5 keV transitions showing evidence of the new transitions populating the 1754.6 keV  $8^-$  level in  $^{148}\text{Ce}$ . New transitions are labeled with an asterisk.

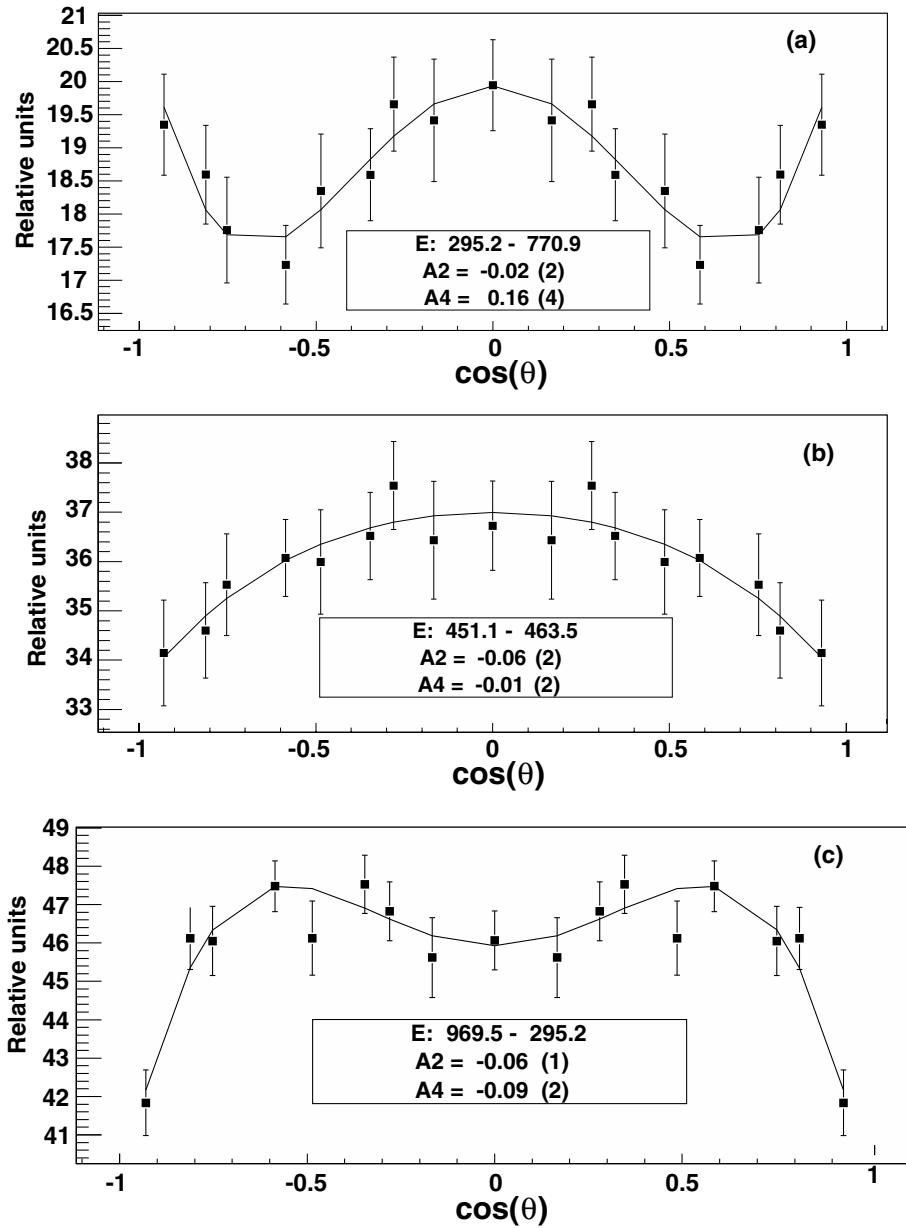


Figure 6: Examples of angular correlation measurements of (a) 295.2 and 770.9 keV cascade, (b) 451.1 and 463.5 keV cascade and (c) 969.5 and 295.2 keV cascade.



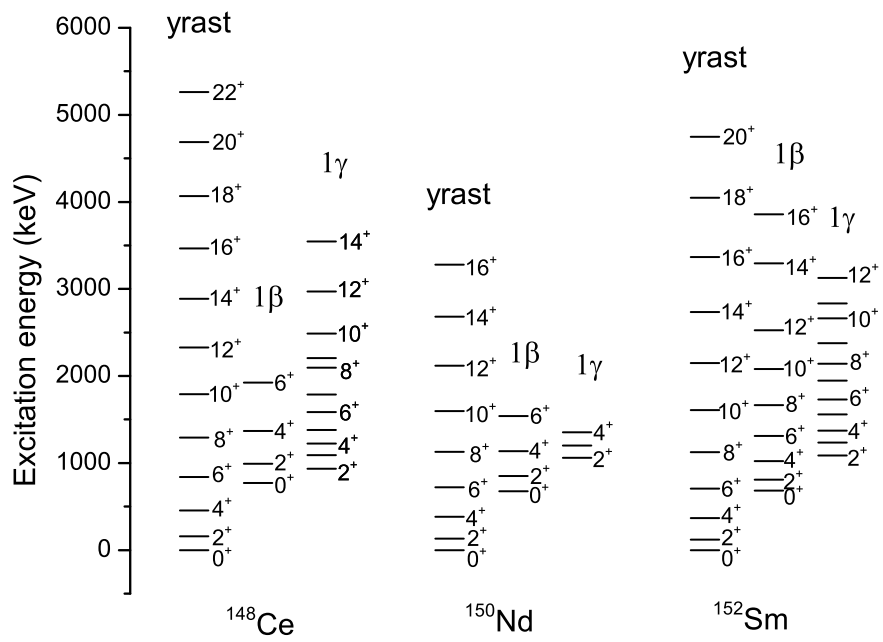


Figure 7: Comparison of the ground state band, the  $1\beta$  and  $1\gamma$  vibrational bands in  $^{148}\text{Ce}$ ,  $^{150}\text{Nd}$  and  $^{152}\text{Sm}$ .

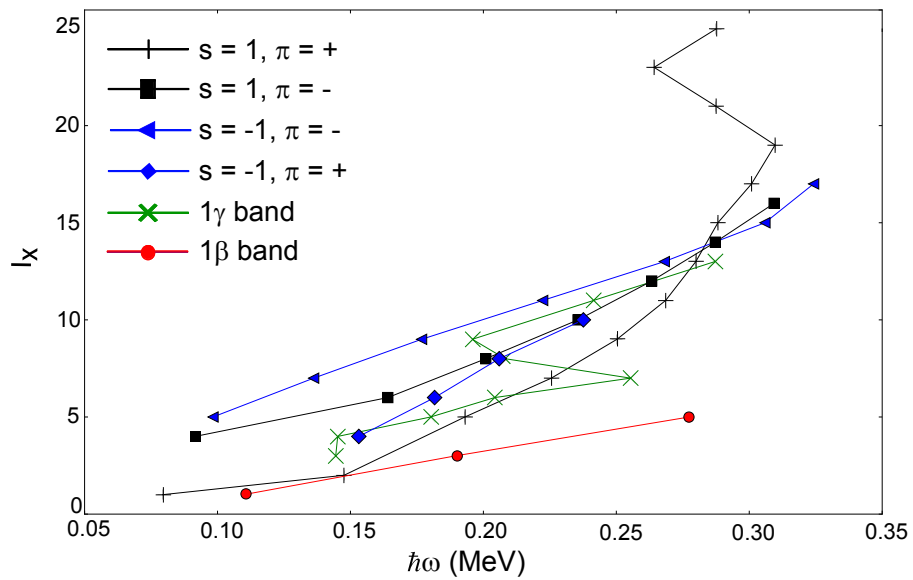


Figure 8: (Color online) Angular momentum alignment vs. rotational frequency of the ground state band, octupole bands, the  $1\beta$  vibrational band and the  $1\gamma$  vibrational band in  $^{148}\text{Ce}$ .

**Declaration of interests**

The authors declare that they have no known competing financial interests or personal relationships that could have appeared to influence the work reported in this paper.

The authors declare the following financial interests/personal relationships which may be considered as potential competing interests:

**E. H. Wang:** Conceptualization, Methodology, Software, Formal analysis, Data Curation, Writing - Original Draft,  
**N. T. Brewer:** Conceptualization, Methodology, Software, Formal analysis, Data Curation, Writing - Original Draft, Visualization,  
**J. H. Hamilton:** Formal analysis, Writing - Review & Editing, Investigation, Supervision, Project administration, Funding acquisition,  
**A. V. Ramayya:** Writing - Review & Editing, Investigation, Supervision, Funding acquisition,  
**W. A. Yzaguirre:** Formal analysis, Writing - Original Draft  
**J. K. Hwang:** Writing - Review & Editing, Investigation,  
**S. H. Liu:** Writing - Review & Editing,  
**Y. X. Luo:** Writing - Review & Editing, Investigation,  
**J. O. Rasmussen:** Writing - Review & Editing, Investigation,,  
**S. J. Zhu:** Writing - Review & Editing, Investigation,  
**G. M. Ter-Akopian:** Writing - Review & Editing, Investigation,  
**Yu. Ts. Oganessian:** Writing - Review & Editing, Investigation.